ASME International
The American Society of Mechanical Engineers
Three Park Avenue
New York, NY 10016-5990

Reprinted From
AD-Vol. 59/MD-Vol. 87, Adaptive Structures and Material Systems
Editor: James Redmond
Book No. G01136 - 1999

Viscothermal damping in thin gas or fluid layers

W.M. Beltman, T.G.H. Basten, H. Tijdeman
University of Twente, Department of Mechanical Engineering,
P.O. Box 217, 7500 AE Enschede, The Netherlands.
w.m.beltman@wb.utwente.nl, t.g.h.basten@wb.utwente.nl, h.tijdeman@wb.utwente.nl

Abstract

This paper deals with viscothermal wave propagation, including acousto-elastic interaction. For wave propagation in thin gas or fluid layers, the effects of viscosity and thermal conductivity have to be accounted for. These effects can introduce a significant dissipation of energy. A model to describe viscothermal wave propagation was developed. It includes the effect of inertia, viscosity, compressibility and thermal conductivity. It was written in terms of dimensionless parameters. These parameters govern the validity of simplifications and they can be used to put models into perspective. The viscothermal model is validated with specially designed experiments. A numerical finite element model was developed that includes the full acousto-elastic coupling. This model was also validated with experiments. The influence of barriers in a thin layers was investigated experimentally. Finally, the new techniques were applied to a number of practical problems: the damping of double wall panels and the dynamical behaviour of a folded array of solar panels during launch.

Nomenclature

C_p	specific heat at constant pressure	J/kgK
C_v	specific heat at constant volume	J/kgK
$\overline{T}$	temperature	K
T	dimensionless temperature amplitude	
T_0	mean temperature	K
c_0	undisturbed speed of sound	m/s
f_n	natural frequency	Hz
$\overline{h}$	layer thickness	m
h_0	half the mean layer thickness	m
h_b	dimensionless displ. amplitude	
h_b	dimensionless displ. amplitude bottom surface	
h_t	dimensionless displ. amplitude top surface	
i	imaginary unit	
k	reduced frequency	
$\overline{p}$	pressure	Pa
p	dimensionless pressure amplitude	
p_0	mean pressure	Pa
s	shear wave number	
t	time	s
$\overline{v}$	velocity vector	m/s
v	dimensionless velocity vector	
$\overline{x}$	x coordinate	m
x	dimensionless coordinate	
$\overline{y}$	y coordinate	m
y	dimensionless coordinate	
$\overline{\rho}$	density	kg/m^3
ρ	dimensionless density amplitude	
ρ_0	mean density	kg/m^3
ω	angular frequency	1/s
γ	ratio of specific heats	
σ	square root of the Prandtl number	
λ	thermal conductivity	W/mK
μ	viscosity	Ns/m^2
η	bulk viscosity	Ns/m^2
ξ	damping coefficient	
ζ	viscosity ratio	
Γ	propagation constant	
$B(s)$	viscous function	
$n(s\sigma)$	polytropic constant	

1 Introduction

Acoustic wave propagation in gases is usually described with the wave equation. The standard wave equation assumes inviscid and adiabatic behaviour. However, when the gas is trapped in a thin layer, boundary layer effects can play an important role. In this case the effects of viscosity and thermal conductivity have to be taken into account. A significant amount of acoustic energy can be dissipated by means of these phenomena.

Several investigations deal with viscothermal wave propagation, see e.g. Rayleigh (1945), Bruneau et al. (1989), Plantier and Bruneau (1990), Karra and Tahar (1997), Moldover et al. (1986), Trochidis (1982), Fox and Whit-

ton (1980), Chow and Pinnington (1987), Önsay (1994), Tijdeman (1975), Beltman (1999a) and Beltman (1999b).

The present paper attempts to give an overview of the research on viscothermal wave propagation in thin gas layers in general and at the University of Twente in particular. Based on an approach with dimensionless parameters, a framework is provided that is used to put the literature on the subject into perspective. For a detailed description, appropriate references are presented. The theory, presented in this paper for wave propagation in thin layers can also be used for thin tubes. For more details, the reader is referred to Tijdeman (1975) and Beltman (1998).

First, a model will be presented to describe viscothermal wave propagation. Based on the use of dimensionless parameters, the most efficient model is identified. The viscothermal models are validated with specially designed experiments. Next, a numerical finite element model is presented that is able to deal with fully coupled acousto-elastic calculations. This model is also experimentally validated. The influence of barriers in a gas layer is studied experimentally. Finally, the theory is applied to a number of practical problems.

2 Viscothermal wave propagation

2.1 Overview

Viscothermal wave propagation is governed by the Navier Stokes equations, the equation of continuity and the equation of state for an ideal gas. Small, dimensionless harmonic perturbations are introduced according to

$$\begin{aligned} \overline{v} &= c_0 v e^{i\omega t} & \overline{p} &= p_0\left[1+pe^{i\omega t}\right] \\ \overline{T} &= T_0\left[1+Te^{i\omega t}\right] & \overline{\rho} &= \rho_0\left[1+\rho e^{i\omega t}\right], \end{aligned} \quad (1)$$

where $\overline{v}$ is the velocity vector, $\overline{p}$ is pressure, $\overline{\rho}$ is density, $\overline{T}$ is temperature, t is time, c_0 is the undisturbed speed of sound, T_0 is mean temperature, p_0 is mean pressure, ρ_0 is mean density, ω is angular frequency and i is the imaginary unit. Based on any additional simplifications that are introduced, three classes of models can be distinguished.

The first type of model is based on a solution of the full set of linearized basic equations. This leads to a relatively complicated set of equations, see e.g. Bruneau et al. (1989), Plantier and Bruneau (1990) and Moldover et al. (1986). Analytical solutions can only be obtained for very simple configurations. Recently, a boundary element method was presented by Karra and Tahar (1997) to deal with more complicated situations.

The second type of model introduces some additional simplifications like incompressibility of the gas, see Trochidis (1982). This leads to a simpler type of model.

The simplest type of model is the third type of model. In these models the pressure is assumed to be constant across the layer thickness. This leads to a very simple and very useful model, see e.g. Fox and Whitton (1980), Önsay (1994), Tijdeman (1975), Beltman (1999a), Basten et al. (1998).

The validity of the models can be expressed in terms of appropriate dimensionless parameters. The following dimensionless parameters govern viscothermal wave propagation in thin gas layers

$$\begin{aligned} \text{shear wave number} \quad & s = h_0\sqrt{\frac{\rho_0\omega}{\mu}} \\ \text{reduced frequency} \quad & k = \frac{\omega h_0}{c_0} \\ \text{ratio of specific heats} \quad & \gamma = \frac{C_p}{C_v} \\ \text{square root of the Prandtl number} \quad & \sigma = \sqrt{\frac{\mu C_p}{\lambda}} \\ \text{viscosity ratio} \quad & \zeta = \frac{\eta}{\mu}\ , \end{aligned} \quad (2)$$

where h_0 is half the layer thickness, μ is viscosity, η is the bulk viscosity, C_p is the specific heat at constant pressure, C_v is the specific heat at constant volume and λ is the thermal conductivity. For monatomic gases $\eta = 0$, for air $\eta = 0.6\mu$.

The shear waver number s, is a measure for the ratio between inertial effects and viscous effects. For large shear wave numbers the effects of viscosity can be neglected compared to the inertial effects, whereas for low shear wave numbers the inertial effects can be neglected compared to the viscous effects. The shear wave numbers can also be interpreted as the ratio between the layer thickness and the boundary layer thickness. The reduced frequency k represents the ratio between the layer thickness and the acoustic wavelength. Typically, the acoustic wave length is very large compared to the layer thickness for viscothermal problems. The third class of models that assume a constant pressure across the layer thickness, are valid for $k/s \ll 1$ and $k \ll 1$. Only under very extreme conditions these conditions are not satisfied. Therefore for most cases these conditions are satisfied and the simplest models are sufficient and the most efficient, see e.g. Beltman (1999a). These models will be referred to as "low reduced frequency models".

2.2 The low reduced frequency model

Consider the squeeze motion that is induced by two parallel surfaces that are vibrating in out-of-plane motion. The distance between the surfaces can be written as

$$\overline{h}(x,y) = h_0\left[2+\left\{h_t(x,y)-h_b(x,y)\right\}e^{i\omega t}\right], \quad (3)$$

where h_0 is half the mean layer thickness, and $h_t(x,y)$ and $h_b(x,y)$ denote the dimensionless displacement amplitudes of the top and the bottom surfaces respectively. Note that the displacement can be a function of the in-plane coordinates x and y. The top and bottom surfaces are assumed to be isothermal. For viscothermal wave propagation in this thin layer, the low reduced frequency model gives the following differential equation for the pressure perturbation

$$\frac{\partial^2 p}{\partial x^2} + \frac{\partial^2 p}{\partial y^2} - \Gamma^2 p = n(s\sigma)\Gamma^2 \frac{1}{2}\left[h_t - h_b\right], \qquad (4)$$

where Γ, $B(s)$ and $n(s\sigma)$ are given by

$$\Gamma = \sqrt{\frac{\gamma}{n(s\sigma)B(s)}}$$

$$n\left(s\sigma\right) = \left[1 + \left[\frac{\gamma - 1}{\gamma}\right] B\left(s\sigma\right)\right]^{-1} \qquad (5)$$

$$B(s) = \frac{\tanh\left(s\sqrt{i}\right)}{s\sqrt{i}} - 1.$$

The dimensionless coordinates x and y are

$$x = \frac{\omega \overline{x}}{c_0} \quad ; \quad y = \frac{\omega \overline{y}}{c_0}. \qquad (6)$$

The differential equation resembles the standard wave equation. The wave number is now a complex, frequency dependent quantity that incorporates the viscous and thermal effects in the propagation constant Γ. The propagation constant is a complex quantity. The real part reflects the attenuation per unit distance, whereas the imaginary part reflects the phase shift per unit distance. The value of Γ is affected by viscous effects, accounted for in $B(s)$, and thermal effects, accounted for in $n(s\sigma)$. Note that the differential equation does not contain any derivatives of the pressure with respect to the out-of-plane z coordinate, since the pressure is assumed constant across the layer thickness. On the right hand side, a source term is present that reflects the squeeze motion that is induced by the vibrating surfaces.

For low shear wave numbers the differential equation reduces to a linearized form of the Reynolds equation. For high shear wave numbers it reduces to a modified form of the wave equation. The modification is due to the fact that the pressure is assumed constant across the layer thickness.

2.3 Experimental validation of the low reduced frequency model

In order to validate the low reduced frequency model, special experiments were carried out with an oscillating solar panel, see Beltman et al. (1997). Consider a rectangular solar panel, suspended in springs at the corners (see Fig.1).

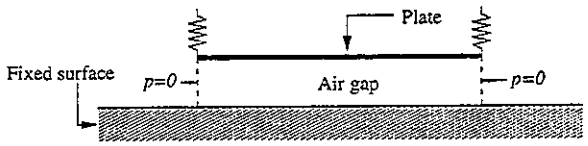

Figure 1: Translating solar panel

The solar panel is located parallel to a fixed surface. The distance between the panel and the fixed surface, the layer thickness, can be adjusted. The panel is excited by an electrodynamic shaker in the centre. It performs a small normal oscillation perpendicular to the fixed surface. The panel is assumed to behave rigidly, and thus the system can be regarded as a simple one degree of freedom mass spring system. The eigenfrequency of the system is affected by the surrounding air and the thin layer in particular. The mass of the panel is 2.54 kg and the dimensions are 0.98 m by 0.98 m. The average stiffness of each of the 8 springs is 1186 N/m. The eigenfrequency in vacuum is 9.7 Hz. Due to the influence of the air, the eigenfrequency and the damping of the system will be affected.

The pressure distribution in the layer can be calculated analytically. The pressure at the edges of the panel is set to zero. The pressure is then solved from Eq.(4), where the dimensionless displacement amplitude of the fixed surface, $h_b = 0$, is zero, and the dimensionless displacement amplitude of the solar panel, h_t is constant: $h_t = h$. The resulting force on the panel is obtained by integration. The influence of the air on the upper side of the panel is neglected in the analytical calculations. This simplification was confirmed by straightforward potential flow calculations for inviscid behaviour. The results from the viscothermal analytical model are compared with finite element results. The finite element calculations are based on standard finite elements, and therefore do not include viscous or thermal effects. This allows a comparison with an approach based on standard acoustic techniques.

The experimental setup is given in Fig.2. The acceleration of the panel is measured in several points to check the rigid behaviour of the panel. The eigenfrequency and the damping coefficient were determined as a function of the layer thickness. The present setup was designed with the help of the dimensionless parameters. The aim of the investigation was to validate the viscothermal wave propagation model. Thus, the shear wave number should be of the order of magnitude of 1. In the literature, experiments are carried out at relatively high frequencies. Consequently, very small gap widths had to be used. These small gap widths are very hard to control. Furthermore, there is a degree of un-

certainty related to the flexibility of the surfaces for these high frequencies. The present investigation deals with a large scale, low frequency approach. The parameters are easy to control and the accuracy of the experiments is very high. The results are given in Fig.3 and Fig.4.

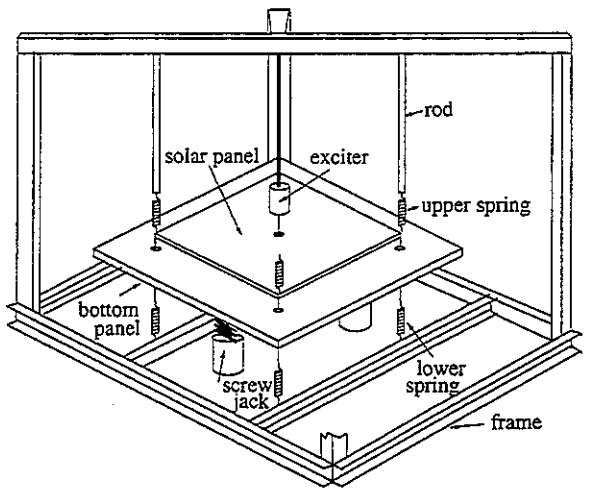

Figure 2: Experimental setup

The eigenfrequency shows a strong decrease with decreasing gap width. The air that is trapped between the panel is subjected to the squeeze motion of the panel. This results in high pressures in the layer. The effect of the air can be interpreted as an added mass effect: the panel behaves as if it were very heavy. The shift in eigenfrequency can be used to extract the amount of added mass. For a layer thickness of 3 mm the added mass is about 23 kg: almost ten times the mass of the panel itself. This illustrates that thin gas layers can have a very important influence on the dynamical behaviour of these lightweigth structures. The agreement between theory and experiments is good. Both the finite element model and the analytical viscothermal model accurately predict the eigenfrequency of the system. In this case the viscothermal effects only have a minor influence on the eigenfrequency of the system.

Viscothermal effects introduce a significant amount of damping in the system. In the present setup, damping values as high as 35% were measured. The viscothermal model is able to predict the damping very well. Note that the standard wave equation models predict zero damping because no dissipative elements are included.

3 Acousto-elastic interaction

In practical applications, one has to deal with a thin layer of gas trapped between vibrating flexible surfaces. Especially

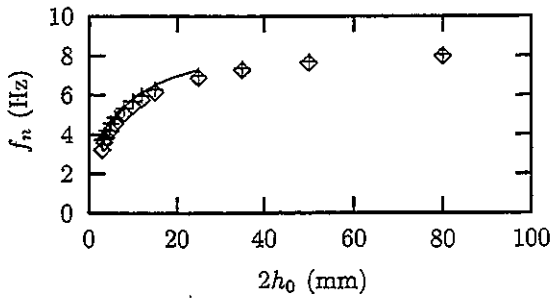

Figure 3: Eigenfrequency versus layer thickness. Low reduced frequency model (—), experiments (◇), finite element model (+)

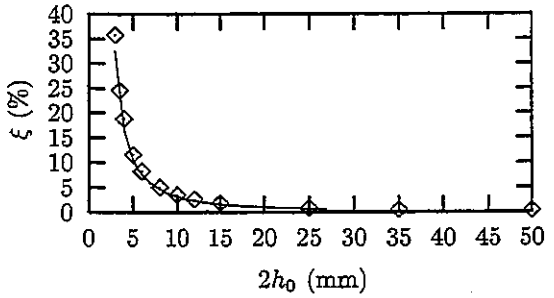

Figure 4: Damping coefficient versus layer thickness. Low reduced frequency model (—), experiments (◇)

for these thin layers there can be a strong coupling and the acousto-elastic interaction has to be accounted for. Analytical solutions can only be found for simple geometries and simple boundary conditions. A finite element model will be presented that is able to deal with fully coupled acousto-elastic calculations including viscothermal wave propagation.

3.1 Structural model

The dynamical behaviour of the structure is written in the following standard finite element formulation:

$$-\omega^2 [M^s] \{U\} + [K^s] \{U\} = [K^c] \{P\} + \{F^{ext}\}, \quad (7)$$

where $[M^s]$ denotes the structural mass matrix, $[K^s]$ is the stiffness matrix, $[K^c]$ is the coupling matrix resulting from the pressure on the interface between structure and gas, and $\{F^{ext}\}$ is the external nodal force vector.

3.2 Viscothermal acoustic model

The starting point for the viscothermal acoustic model is the low reduced frequency Eq.(4). Because of the similarity with the standard wave equation, a finite element model can

be constructed in a very straightforward way. This finally gives, see Beltman et al. (1998):

$$-\omega^2 [M^a(s)] \{P\} + [K^a] \{P\} = \omega^2 [M^c(s)] \{U\}, \quad (8)$$

where $[M^a(s)]$ denotes the acoustic mass matrix, $[K^a]$ is the acoustic stiffness matrix, $\{P\}$ is the vector with the nodal pressure degrees of freedom, $\{U\}$ is the vector with the nodal structural degrees of freedom and $[M^c(s)]$ is the coupling matrix. Not that some matrices are complex and frequency dependent.

3.3 Acousto-elastic interaction

In an acousto-elastic calculation, the motion of the structure is coupled to the motion of the gas. On the interface, the normal velocity of the gas is equal to the velocity of the structure. The finite element models of the structure are now coupled:

$$- \omega^2 \begin{bmatrix} [M^s] & [0] \\ [M^c(s)] & [M^a(s)] \end{bmatrix} \begin{Bmatrix} \{U\} \\ \{P\} \end{Bmatrix} + \begin{bmatrix} [K^s] & -[K^c] \\ [0] & [K^a] \end{bmatrix} \begin{Bmatrix} \{U\} \\ \{P\} \end{Bmatrix} = \begin{Bmatrix} \{F^{ext}\} \\ \{0\} \end{Bmatrix}. \quad (9)$$

This system contains the mass matrices and the stiffness matrices of the structural part and the acoustic part. The coupling is established by the two coupling matrices, $[M^c(s)]$ and $[K^c]$. These matrices are related by

$$[M^c(s)] = \frac{\rho_0}{h_0 B(s)} [K^c]^T. \quad (10)$$

3.4 Experimental validation of the acousto-elastic model

The acousto-elastic finite element model was experimentally validated with a setup that was first described by Dowell et al. (1977). A rectangular aluminium plate is clamped at the edges in an aluminum frame (see Fig.5). In the box there is a thick bottom plate parallel to the thin aluminum plate. The distance between the bottom and the plate can be varied, thus entrapping a layer of air. The eigenfrequencies and the damping coefficients of the coverplate are calculated and measured as a function of the layer thickness $2h_0$. In the calculations, a mesh consisting of 20 x 20 plate elements was used. These elements were coupled to 20 x 20 viscothermal acoustic finite elements with interface elements.

The measured and calculated eigenfrequencies as a function of the layer thickness are given in Fig. 6. The modes are identified by the half number of wavelengths in the x and y direction in vacuum respectively. For example, 11 is the first mode of a clamped plate in vacuum, with one

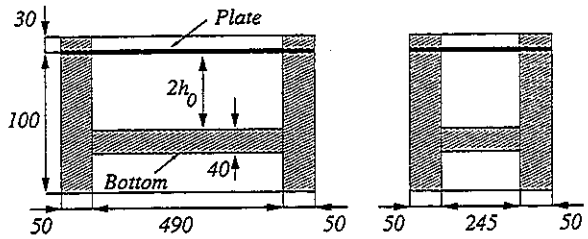

Figure 5: Airtight box with flexible coverplate

half wavelength in the x direction, and one half wavelength in the y direction. In general, the agreement between calculated results and experimental results is good. For the higher modes the numerical results start to deviate due to the limited number of elements, but in total the agreement is very satisfactory.

The figure shows that the eigenfrequencies of the coverplate change dramatically as a function of the layer thickness. There even are some cross overs. This example illustrates the need for a coupled analysis. The behaviour of the coupled system is totally different than the behaviour of the uncoupled systems. For instance, the eigenfrequencies and the mode shapes of the plate change as a function of the layer thickness. An analysis based on the uncoupled behaviour of the plate thus gives wrong results.

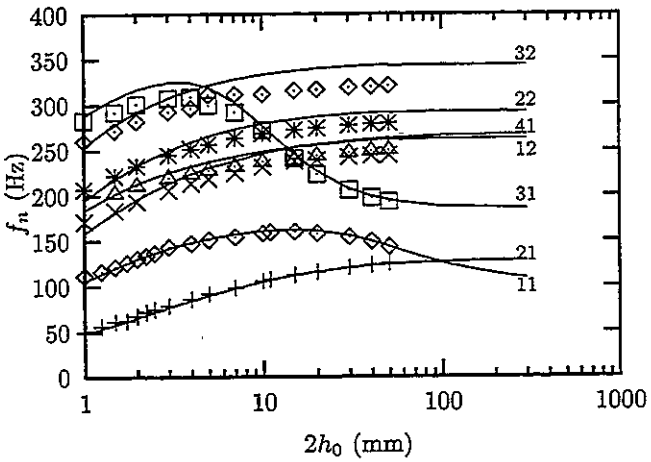

Figure 6: Eigenfrequencies of airtight box with flexible coverplate. Lines: calculations. Symbols: experiments.

Fig.6 shows two different types of behaviour. Mode 11 and mode 31 first show an increase in frequency with decreasing gap width. The other modes all show a steady decrease in eigenfrequency with decreasing gap width. The different behaviour can be explained in terms of added mass and added stiffness. In general, the motion of the coverplate

induces a squeeze effect in the air. The pumping of air in the layer is experienced by the plate as an added mass. This effect increases as the layer thickness decreases, as was also observed in the previous experiments. Therefore the eigenfrequencies decrease with decreasing layer thickness.

The modes 11 and 31 are symmetric modes. For these modes, the displacement of the coverplate is accompanied by a net change in cavity volume. The change in volume is experienced by the plate as an added stiffness. For a closed volume, the added stiffness effect can be very strong. The pressure disturbance due to the net volume change increases as the layer thickness decreases. Therefore the frequencies increase with decreasing layer thickness. However, the mode shapes also change in this process. In fact, as the layer thickness decreases these symmetric modes tend to take a shape which induces a zero net volume change. In that case the added stiffness effect decreases again and the added mass effect starts to dominate. The change in modeshape explains the behaviour in eigenfrequency as a function of the layer thickness.

The damping coefficient for the modes 11 and 21 are given in Fig.7. The damping shows a strong increase with decreasing layer thickness. The damping is mainly induced by viscous shear and is related to the pumping of air in the layer. The 21 mode is an asymmetric mode that pumps the air efficiently. Therefore the damping is especially high for this mode. The agreement between experiments and calculations is good. The present analysis only gives a brief overview of the most important techniques and observations. For an extensive discussion the reader is referred to Beltman et al. (1998) and Beltman (1998).

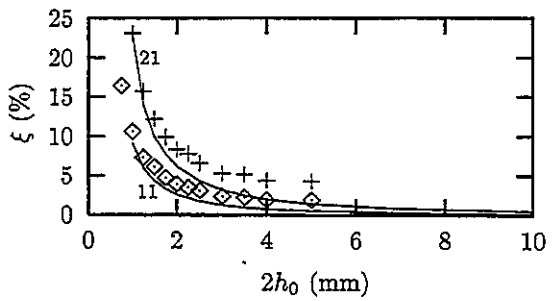

Figure 7: Damping coefficients of airtight box with flexible coverplate. Lines: calculations. Symbols: experiments.

4 Barriers in a layer

In many practical applications, the airflow in a layer is (partly) obstructed by barriers in the layer like ribs or cables. In order to investigate the influence of barriers, experiments were carried out with the oscillating solar panel.

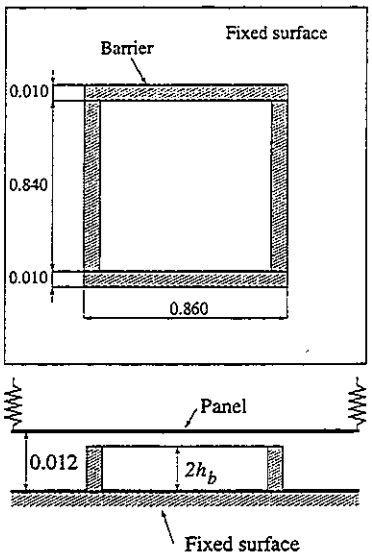

Figure 8: Barriers obstructing the airflow. Top view and side view.

Barriers were placed in the layer between the panel and the fixed surface (see Fig.8). The barriers have a rectangular cross section and obstruct the airflow. A small gap remains between the oscillating panel and the top of the barriers. In the experiments, a layer thickness of 12 mm was used and experiments were carried out with barrier heights of 10.66, 10.33, 10.00, 9.00 and 8.00 mm. Eigenfrequency and damping of the system were measured and special attention was paid to the linearity of the response.

In the experiments, the flow around the barriers was visualised with smoke tests. A vortex was present during the outflow stage of the vibration cycle. Fig.9 shows the vortex for a barrier height of 10.66 mm.

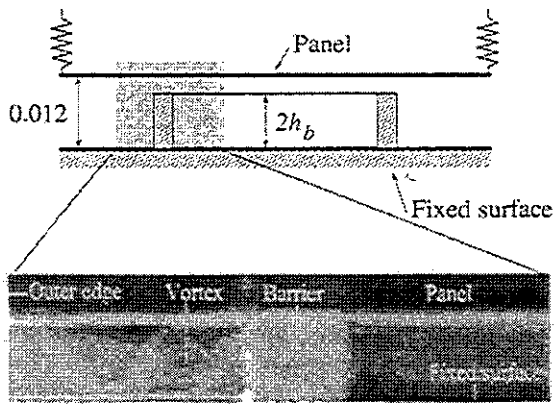

Figure 9: Vortex

The vortex is due to nonsteady flow separation at the trailing edge of the barrier. It introduces a strong nonlinear dissipative behaviour. The eigenfrequency of the system is not affected very much by the presence of the vortex, but the damping coefficient is now a function of the displacement amplitude of the panel. In Fig.10 the damping coefficient is plotted versus the displacement amplitude $h_0 h$ for a barrier height of 10.66 mm. The figure shows that the damping coefficient is approximately a linear function of the displacement amplitude. This behaviour can be explained with a simple model. The dissipation on energy in an open ended pipe was investigated by Disselhorst and van Wijngaarden (1980) and Peters et al. (1993). They developed a simple model, based on a theoretical and experimental analysis. The model describes the dissipation of energy that is caused by nonsteady flow separation at the open end of a pipe. This model is now used to estimate the damping coefficient for the present configuration. The results are given in Fig.10. The agreement between the simple approximate model and the experimental values is remarkable. For a more detailed discussion the reader is referred to Beltman (1998).

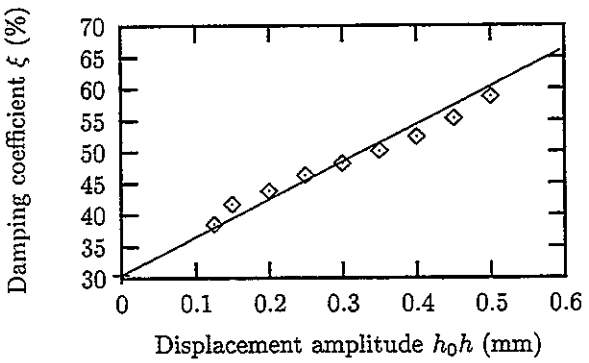

Figure 10: Damping coefficient versus displacement amplitude. Line: calculation with simple model. Symbols: experiments.

5 Practical applications

5.1 Solar panels during launch

During the launch phase the solar panels are folded against the body of the satellite (see Fig.11). Thin layers of air are trapped between the lightweigth panels. During launch the satellite and the solar panels in the payload fairing are exposed to severe structural and acoustic loads. In order to function properly, any damage to the solar panels or the satellite must be avoided. The dynamical behaviour of the folded array of solar panels is thus very important. Before a satellite is launched, the folded pack of solar panels is subjected to several structural and acoustic tests. For instance, a sine sweep base excitation in carried out in the frequency range between 10 and 100 Hz. These experiments have shown that the air layers between the panels have an important influence on the dynamical behaviour. In cooperation with Fokker Space, a series of studies was carried out. The new acousto-elastic techniques, including viscothermal wave propagation, were used to construct a model of a complete folded solar array. Eigenfrequencies, damping values and loads were calculated and compared with experimental values. The models are now an important tool in the design of solar panels.

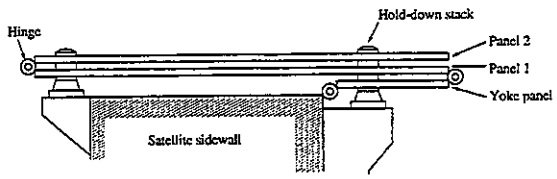

Figure 11: SOHO (SOlar and Heliospheric Observatory) wing in stowed position, side view

5.2 Damping of double wall panels: a demonstrator

A second application of the new techniques is the damping of double wall panels. The previous investigations have shown that a significant amount of energy can be dissipated in a thin gas layer by means of viscous shear. The amount of energy that is dissipated is related to the pumping of air. With the new models, an optimization can be carried out to obtain high damping values. For a double wall panel system, consisting of two flexible aluminium plates separated by a thin air layer, a demonstrator was constructed. The plates were designed in such a way that a high amount of energy is dissipated in the layer. On the one hand, the layer has to be thin because the viscous dissipation increases with decreasing layer thickness. On the other hand, the coupling between the panels increases as the distance decreases. If the coupling is very strong, both plates move in phase and no squeeze motion is induced in the layer. Calculations have shown that for the present configuration a plate thickness ratio of 1:2 is optimal.

The demonstrator consists of two parallel aluminium plates that are clamped at the edges (see Fig.12). The dimensions of the panels are 0.49 x 0.245 m. Plates with different thicknesses can be used. The distance between the panels can be adjusted. One plate is excited with an electrodynamic shaker. The acceleration, input force and the phase angle between force and acceleration are measured and used to keep the power input to the system constant

if the layer thickness is changed. When the layer thickness decreases, the dissipation of energy in the layer causes less sound to be radiated from the plates. This effect can be heard very clearly. In order to quantify this effect, the radiated power was determined with sound intensity measurements (see Fig.13). If the layer thickness is very small, almost all the input power is dissipated in the layer. Consequently, little sound is radiated from the plates.

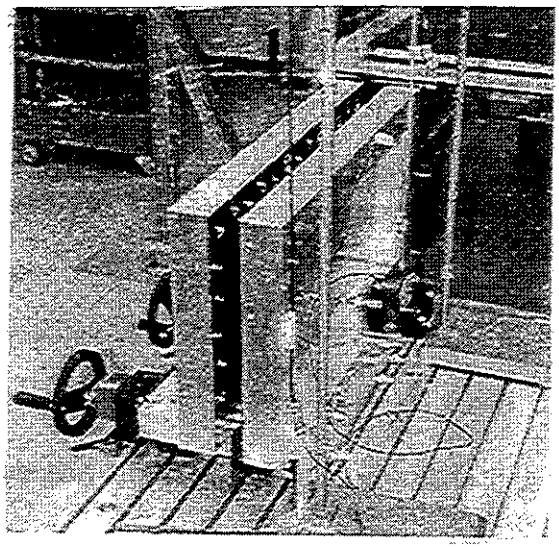

Figure 12: Demonstrator for the damping of double wall panels

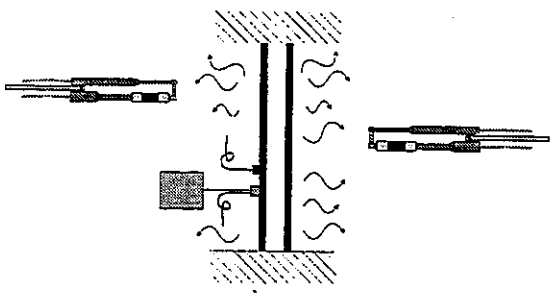

Figure 13: Intensity measurements for double wall panels

Conclusions

Models were developed to describe viscothermal wave propagation in thin gas or fluid layers, including acousto-elastic interaction. The models were validated with specially designed experiments. Calculations and experiments show good agreement. The investigations demonstrate that a significant amount of energy can be dissipated in a thin gas layer by means of viscous shear. The damping can be further increased by placing barriers in the layer. This introduces a strong nonlinear dissipation because of the unsteady flow separation. The models were successfully applied to a number of practical problems.

Acknowledgments

The authors thank Ruud Spiering, Peter van der Hoogt, Bert Wolbert, Frits van der Eerden and Marco Oude Nijhuis for their help, comments and suggestions. The support of Shell, Fokker Space and the National Aerospace Laboratory is gratefully acknowledged. This research is supported by the Technology Foundation (STW).

References

Basten, T., W. Beltman, and H. Tijdeman, 1998. Optimization of viscothermal damping of double wall panels. In *InterNoise 98*, Christchurch, New Zealand.

Beltman, W., 1998. *Viscothermal wave propagation including acousto-elastic interaction.* Ph. D. thesis, University of Twente, Department of Mechanical Engineering, The Netherlands. ISBN 90-3651217-4.

Beltman, W., 1999a, November. Viscothermal wave propagation including acousto-elastic interaction, part I: theory. *Journal of Sound and Vibration.*

Beltman, W., 1999b, November. Viscothermal wave propagation including acousto-elastic interaction, part II: applications. *Journal of Sound and Vibration.*

Beltman, W., P. van der Hoogt, R. Spiering, and H. Tijdeman, 1997. Air loads on a rigid plate oscillating normal to a fixed surface. *Journal of Sound and Vibration 206*(3), 217–241.

Beltman, W., P. van der Hoogt, R. Spiering, and H. Tijdeman, 1998. Implementation and experimental validation of a new viscothermal acoustic finite element for acousto-elastic problems. *Journal of Sound and Vibration 216*(1), 159–185.

Bruneau, M., P. Herzog, J. Kergomard, and J. Polack, 1989. General formulation of the dispersion equation in bounded visco-thermal fluid. *Wave Motion 11*, 441–451.

Chow, L. and R. Pinnington, 1987. Practical industrial method of increasing structural damping in machinery, I: squeeze film damping with air. *Journal of Sound and Vibration 118*, 123–139.

Disselhorst, J. and L. van Wijngaarden, 1980. Flow in the exit of open pipes during acoustic resonance. *Journal of Fluid Mechanics 99*, 293–319.

Dowell, E., G. Gorman, and D. Smith, 1977. Acousto-elasticity: general theory, acoustic natural modes and forced response to sinusoidal excitation, including comparisons with experiment. *Journal of Sound and Vibration 52*, 519–542.

Fox, M. and P. Whitton, 1980. The damping of structural vibrations by thin gas films. *Journal of Sound and Vibration 73*, 279–295.

Karra, C. and M. B. Tahar, 1997. An integral equation formulation for boundary element analysis of propagation in viscothermal fluids. *Journal of the Acoustical Society of America 102*(3), 1311–1318.

Moldover, M., J. Mehl, and M. Greenspan, 1986. Gas-filles spherical resonators: theory and experiment. *Journal of the Acoustical Society of America 79*, 253–270.

Önsay, T., 1994. Dynamic interaction between the bending vibrations of a plate and a fluid layer attenuator. *Journal of Sound and Vibration 178*, 289–313.

Peters, C., A. Hirschberg, A. Reijen, and A. Wijnands, 1993. Damping and reflection coefficient measurements for an open pipe at low Mach and low Helmholtz numbers. *Journal of Fluid Mechanics 256*, 499–534.

Plantier, G. and M. Bruneau, 1990. Heat conduction effects on the acoustic response of a membrane separated by a very thin air film from a backing electrode. *Journal Acoustique 3*, 243–250.

Rayleigh, J., 1945. *The Theory of Sound* (second, revised ed.), Volume II. Dover publications.

Tijdeman, H., 1975. On the propagation of sound waves in cylindrical tubes. *Journal of Sound and Vibration 39*, 1–33.

Trochidis, A., 1982. Vibration damping due to air or liquid layers. *Acustica 51*, 201–212.